Journal of Organometallic Chemistry, 365 (1989) 163–185
Elsevier Sequoia S.A., Lausanne – Printed in The Netherlands
JOM 09637

Relationships between structure and ligand dynamics

II *. Alkyne and carbonyl dynamics in $Os_3(CO)_9$(alkyne)(L) (L = CO, PR_3) **

Edward Rosenberg *, **Julia Bracker-Novak,**

Department of Chemistry, California State University, Northridge, Northridge, California 91330 (U.S.A.)

Robert W. Gellert *

Department of Chemistry and Biochemistry, California State University, Los Angeles, Los Angeles, California 90032 (U.S.A.)

Silvio Aime, Roberto Gobetto *, and Domenico Osella**

Departimento di Chimica Inorganica, Fisica ed Materiale, Universitá di Torino, via P. Giuria 9, Torino (Italy)

(Received July 28th, 1988)

Abstract

The synthesis of the phosphine substituted complexes $Os_3(CO)_9(\mu_3\text{-}\eta^2\text{-}CH_3CH_2\text{-}C{\equiv}CCH_2CH_3)L$ ($L = P(C_6H_5)_3$ (III), $P(CH_3)_3$ (IV)) and $Os_3(CO)_9(\mu_3\text{-}\eta^2\text{-}CH_3C{\equiv}CCH_3)L$ ($L = P(OCH_3)_3$ (V)) are reported. A detailed analysis of the VT-^{1}H and VT-^{13}C NMR of these complexes is presented and compared with the same studies on the parent complexes $Os_3(CO)_9(\mu_3\text{-}\eta^2\text{-}RC{\equiv}CR)(\mu\text{-}CO)$ ($R = CH_2CH_3$ (I), CH_3 (II)). In the parent complexes I and II a two stage exchange process is observed: (1) a low energy process involving axial radial exchange at the carbonyl bridged osmium atoms, (2) a higher energy exchange process in which alkyne motion over the face of the metal triangle is coupled with bridge-terminal exchange of the carbonyls, and with axial–radial exchange at the unique osmium atom. The phosphine derivatives III–V, all show a three stage exchange process: (1) a localized axial-radial exchange at the unsubstituted osmium atoms; (2) a semibridging terminal carbonyl exchange at the phosphine substituted osmium coupled with a restricted oscillation of the alkyne, pivoted on this osmium atom; (3) free motion of the alkyne and averaging of all the carbonyl groups. The relationship between the

* For part I see ref. 2.
** Dedicated to the memory of Prof. J.J. Zuckerman.

0022-328X/89/$03.50 © 1989 Elsevier Sequoia S.A.

differences in the observed dynamic processes are understood by a comparison of the solid state structures of I and III which are also reported. Compound I crystallizes in the triclinic space group $P\bar{1}$, with unit cell parameters a 9.292(2), b 15.340(3), c 8.391(2) Å, α 91.27(2), β 116.70 (1), γ 105.24(2)°, V 1017.3(4) Å^3, and $Z = 2$. Compound III belongs to the monoclinic space group $P2_1/c$, with a 14.271(4), b 11.370(2), c 21.192(5) Å, β 104.43(2)^3, V 3330(1) Å^3, and $Z = 4$. The structures were refined by full matrix least squares to $R_F = 0.044$, $R_{wF} = 0.058$ for I, and $R_F = 0.033$, $R_{wF} = 0.041$ for III, respectively.

Introduction

Previous work on the reactivity of small organic molecules with $Ru_3(CO)_{12}$ and $Os_3(CO)_{12}$ has yielded a plethora of M_3-ligand bonding frameworks [1]. We have been trying to understand the relationship between the structure, reactivity and ligand dynamics in these systems [2,3,4]. In the case of C_2M_3 and C_3M_3 bonding frameworks involving $5e^-$ donor organic fragments we have found that the metal carbon frameworks are relatively rigid compared to the carbonyls and hydrides and have related the cluster's overall ligand dynamics to the subsequent reactions of these fragments on the M_3 clusters [2–5]. On the other hand, we and others have found that in the C_2M_3 clusters with $4e^-$ donor organic fragments the organic ligand is relatively mobile [6,7]. In the particular case of saturated ($48e^-$) $Os_3(CO)_{10}$(alkyne) complexes the relationship between alkyne motion and carbonyl migrations has not been elucidated [7,8]. Only one solid state structure, $Os_3(CO)_{10}(\mu_3\text{-}\eta^2\text{-}C_6H_5C{\equiv}CC_6H_5)$, of this structural type has been reported to date [8]. Indeed the structure of $Os_3(CO)_{10}(\mu_3\text{-}\eta^2\text{-}C_6H_5C{\equiv}CC_6H_5)$ appears to be an exception to the general family of $Os_3(CO)_{10}(4e^-$-alkyne) complexes. Spectroscopic evidence for the family of complexes $Os_3(CO)_{10}(\mu_3\text{-}\eta^2\text{-}RC{\equiv}CR)$ (R = CH_3, CH_2CH_3, H) [7] suggest a structure in which the alkyne is parallel to one edge of the Os_3 triangle and in which there is a symmetrical carbonyl bridge on the edge to which the alkyne is parallel (see structure **A** below). The diphenyl acetylene derivative, however, has a structure in which the alkyne is slightly twisted away from a parallel orientation and in which there are two asymmetric carbonyl bridges with the shorter Os–CO bond length on the osmium atom with the longer M–C(alkyne) bond distance (see structure **B** below).

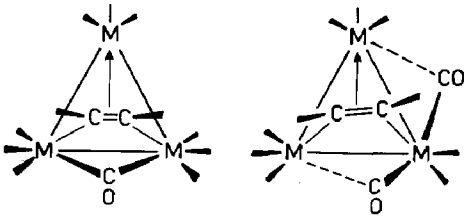

(A) (B)

We report here the solid state structures of the complexes $Os_3(CO)_9(\mu_3\text{-}\eta^2\text{-}CH_3CH_2C{\equiv}CCH_2CH_3)L$ (L = μ-CO, $P(C_6H_5)_3$) in which the transformation from a structure like **A** to a structure like *B* is observed on replacing CO with a

phosphine. Furthermore, we have been able to elucidate the relationship between alkyne and carbonyl migrations in this series and to relate the observed changes in ground state structure within the series to changes in their ligand dynamics.

Results and Discussion

A. Synthesis

The alkyne complexes $Os_3(CO)_9(\mu_3\text{-}\eta^2\text{-}RC{\equiv}CR)(\mu\text{-}CO)$ ($R = CH_3$, CH_2CH_3) were obtained from the room temperature reaction of $H_2Os_3(CO)_{10}$ with an excess of the corresponding alkyne [7]. In both cases ($R = CH_3$, CH_2CH_3) the alkyne complex was the major product and the only one isolated in sufficient yield to allow full characterization [7].

The monophosphine derivatives $Os_3(CO)_9(\mu_3\text{-}\eta^2\text{-}RC{\equiv}CR)L$ ($R = CH_3$, CH_2CH_3, $L = P(C_6H_5)_3$, $P(OCH_3)_3$, and $P(CH_3)_3$) were obtained as the only products from the reactions of the corresponding phosphine with the alkyne complex in refluxing cyclohexane for 3 to 4 h. In all cases the compounds were characterized by variable temperature (VT) -^{13}C and -^{1}H NMR, infrared spectroscopy and elemental analysis (Tables 1, 2 and 4). In the case where $R = CH_2CH_3$, and $L = CO$ and $P(C_6H_5)_3$ we have also determined the solid state structures of these complexes by single crystal X-ray diffraction methods.

Table 1

Low temperature limiting ^{1}H NMR data for $Os_3(CO)_9(\mu_3\text{-}\eta^2\text{-alkyne})L$ complexes ($L = \mu\text{-CO}$, PR_3) [a]

Compound	Alkyne		Substituent	
	$\delta(CH_2)$	$\delta(CH_3)$	$\delta(CH_3)$	$\delta(C_6H_5)$
$Os_3(CO)_9(\mu_3\text{-}\eta^2\text{-}C_2(CH_3CH_2)_2)(\mu\text{-CO})$ (I)	2.76(1,m) 2.17(1,m) (J_{AB} 14.1 Hz)	1.61(3,t) (J_{AX} 6.9 Hz)		
$Os_3(CO)_9(\mu_3\text{-}\eta^2\text{-}C_2(CH_3)_2)(\mu\text{-CO})$ (II)		2.43(3,s)		
$Os_3(CO)_9(\mu_3\text{-}\eta^2\text{-}C_2(CH_3CH_2)_2)(PPh_3)$ (III)	3.09(1,m) (^3J(P–H) 3.0 Hz) 3.03(1,m) 2.84(1,m) 2.44(1,m) (J_{AB} 14.0 Hz)	1.45(3,t) 1.37(3,t) (J_{AX} 7.0 Hz)		7.52(5,m)
$Os_3(CO)_9(\mu_3\text{-}\eta^2\text{-}C_2(CH_3CH_2)_2)(P(CH_3)_3)$ (IV)	2.97(1,m) 2.76(1,m) 2.65(1,m) 2.33(1,m) (J_{AB} 14.0 Hz)	1.37(3,t) 1.21(3,t) (J_{AX} 7.0 Hz)	1.02(9,d)	
$Os_3(CO)_9(\mu_3\text{-}\eta^2\text{-}C_2(CH_3)_2)(P(OCH_3)_3)$ (V)		2.37(3,s) 2.41(3,s)	3.72(9,d)	

[a] Shifts reported downfield positive with respect to TMS in $CDCl_3$. Numbers in brackets are relative intensity, m, multiplet; t, triplet; d, doublet.

Table 2

Carbonyl group infrared stretching frequencies, carbon and hydrogen analyses for $Os_3(CO)_9(\mu_3\text{-}\eta^2\text{-alkyne})L$ complexes, ($L = \mu\text{-CO}$, PR_3), in cyclohexane

Compound [a]	Terminal (ν(CO) (cm^{-1}))	Bridging of semi-bridging ν(CO) (cm^{-1})	Analysis (Found (calcd.) (%))	
			C	H
I	2097 w, 2058 vs 2048 sh, 2025 s 2009 m, 1997 m	1845 w/br	21.05 (20.60)	1.15 (1.07)
II	2098 w, 2057 vs 2045 sh, 2022 s 2007 m, 1998 m	1843 w/br	18.51 (18.38)	0.93 (0.65)
III	2073 m, 2036 vs 2007 s, 1999 vs 1982 s, 1970 m	1950 m 1944 m	33.75 (33.94)	2.39 (2.16)
IV	2072 m, 2033 vs 2010 s, 1997 vs 1985 sh, 1972 m	1955 m 1945 m	22.30 (22.02)	1.69 (1.95)
V	2070 m, 2035 vs 2009 s, 1997 vs 1985 sh, 1973 m	1956 m 1946 m	19.52 (19.19)	1.41 (1.51)

[a] I = $Os_3(CO)_9(\mu_3\text{-}\eta^2\text{-}C_2(CH_3CH_2)_2)(\mu\text{-CO})$, II = $Os_3(CO)_9(\mu_3\text{-}\eta^2\text{-}C_2(CH_3)_2)(\mu\text{-CO})$, III = $Os_3(CO)_9(\mu_3\text{-}\eta^2\text{-}C_2(CH_3CH_2)_2)(PPh_3)$, IV = $Os_3(CO)_9(\mu_3\text{-}\eta^2\text{-}C_2(CH_3CH_2)_2)(P(CH_3)_3)$, and V = $Os_3(CO)_9(\mu_3\text{-}\eta^2\text{-}C_2(CH_3)_2)(P(OCH_3)_3)$.

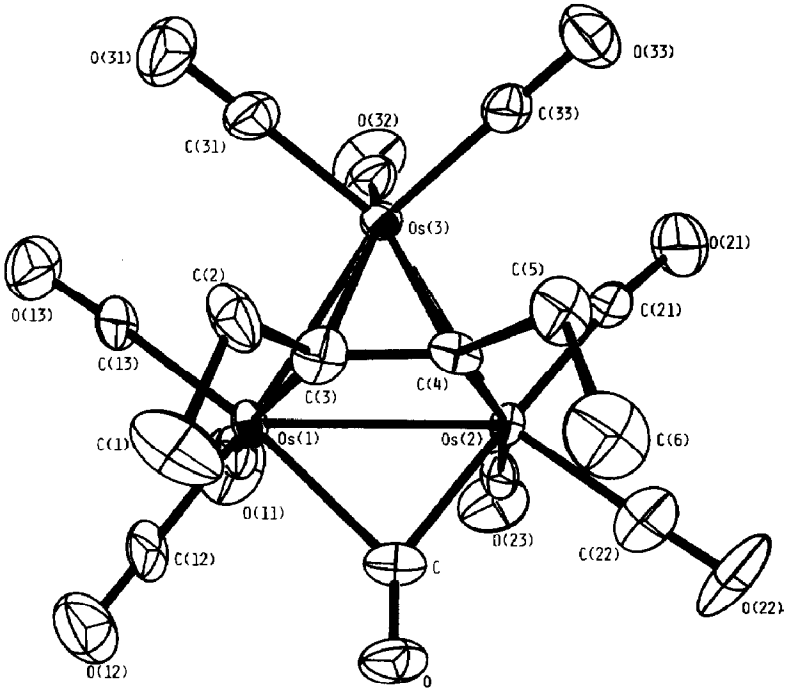

Fig. 1. Ortep illustration of the trimetallic cluster $Os_3(CO)_{10}((CH_3CH_2)_2C_2)$ (I). Thermal ellipsoids are drawn at the 50% probability level.

Table 3

Interatomic distances (Å) and angles (deg) in (I) [a]

Distances			
Os(1)–Os(2)	2.832(1)	Os(3)–C(4)	2.244(16)
Os(1)–Os(3)	2.755(1)	Os(3)–C(3)	2.276(18)
Os(2)–Os(3)	2.763(1)	C–O	1.128(22)
Os(1)–C(11)	1.874(21)	C(11)–O(11)	1.222(28)
Os(1)–C(13)	1.890(19)	C(12)–O(12)	1.124(28)
Os(1)–C(12)	1.906(22)	C(13)–O(13)	1.128(24)
Os(1)–C(3)	2.127(20)	C(21)–O(21)	1.143(27)
Os(1)–C	2.302(18)	C(22)–O(22)	1.131(26)
Os(2)–C(23)	1.900(18)	C(23)–O(23)	1.170(25)
Os(2)–C(22)	1.914(20)	C(31)–O(31)	1.143(23)
Os(2)–C(21)	1.930(20)	C(32)–O(32)	1.119(26)
Os(2)–C	2.086(20)	C(33)–O(33)	1.152(27)
Os(2)–C(4)	2.164(16)	C(1)–C(2)	1.579(32)
Os(3)–C(33)	1.874(21)	C(2)–C(3)	1.502(27)
Os(3)–C(31)	1.882(18)	C(4)–C(5)	1.550(29)
C(3)–C(4)	1.378(27)	C(5)–C(6)	1.556(29)
Os(3)–C(32)	1.918(22)		
Angles			
Os(3)–Os(1)–Os(2)	59.27(2)	C(12)–Os(1)–Os(3)	154.2(6)
Os(3)–Os(2)–Os(1)	58.97(2)	C(12)–Os(1)–Os(2)	124.6(6)
Os(1)–Os(3)–Os(2)	61.76(2)	C(3)–Os(1)–C	82.1(7)
C(11)–Os(1)–C(13)	90.2(8)	C(3)–Os(1)–Os(3)	53.8(5)
C(11)–Os(1)–C(12)	94.7(9)	C(3)–Os(1)–Os(2)	70.9(5)
C(11)–Os(1)–C(3)	162.6(8)	Os(3)–Os(1)–C	102.6(6)
C(11)–Os(1)–C	95.2(7)	Os(2)–Os(1)–C	46.5(5)
C(11)–Os(1)–Os(3)	110.8(6)	C(23)–Os(2)–C(22)	97.5(8)
C(11)–Os(1)–Os(2)	94.7(6)	C(23)–Os(2)–C(21)	89.6(8)
C(13)–Os(1)–C(12)	92.9(9)	C(23)–Os(2)–C	87.9(8)
C(13)–Os(1)–C(3)	95.3(8)	C(23)–Os(2)–C(4)	163.4(8)
C(13)–Os(1)–C	170.0(8)	C(23)–Os(2)–Os(3)	117.5(5)
C(13)–Os(1)–Os(3)	83.3(6)	C(23)–Os(2)–Os(1)	94.0(6)
C(13)–Os(1)–Os(2)	141.5(6)	C(22)–Os(2)–C(21)	93.1(9)
C(12)–Os(1)–C(3)	101.6(8)	C(22)–Os(2)–C	85.4(9)
C(12)–Os(1)–C	78.3(8)	C(22)–Os(2)–C(4)	96.4(7)
C(22)–Os(2)–Os(3)	142.2(7)	C(3)–Os(3)–Os(2)	70.4(4)
C(22)–Os(2)–Os(1)	136.6(7)	C(3)–Os(3)–Os(2)	70.4(4)
C(21)–Os(2)–C	176.9(7)	Os(2)–C–O	144.3(17)
C(21)–Os(2)–C(4)	98.8(7)	Os(1)–C–O	135.4(17)
C(21)–Os(2)–Os(3)	74.3(5)	Os(2)–C–Os(1)	80.2(6)
C(21)–Os(2)–Os(1)	128.9(5)	O(11)–C(11)–Os(1)	176.6(18)
C(4)–Os(2)–C	84.0(7)	O(12)–C(12)–Os(1)	178.4(20)
Os(3)–Os(2)–C	108.5(5)	O(13)–C(13)–Os(1)	175.4(19)
Os(1)–Os(2)–C	53.2(5)	O(21)–C(21)–Os(2)	172.0(14)
C(4)–Os(2)–Os(3)	52.5(4)	O(22)–C(22)–Os(2)	177.6(21)
C(4)–Os(2)–Os(1)	69.5(5)	O(23)–C(23)–Os(2)	178.7(18)
C(33)–Os(3)–C(31)	90.8(8)	O(31)–C(31)–Os(3)	177.0(20)
C(33)–Os(3)–C(32)	98.5(9)	O(32)–C(32)–Os(3)	176.8(17)
C(33)–Os(3)–C(4)	88.9(7)	O(33)–C(33)–Os(3)	177.8(15)
C(33)–Os(3)–C(3)	113.5(8)	C(3)–C(2)–C(1)	110.0(16)
C(33)–Os(3)–Os(1)	159.0(5)	C(4)–C(3)–C(2)	123.9(18)
C(33)–Os(3)–Os(2)	104.0(5)	C(4)–C(3)–Os(1)	109.8(12)
C(31)–Os(3)–C(32)	93.4(8)	C(4)–C(3)–Os(3)	71.0(10)
C(31)–Os(3)–C(4)	116.1(7)	C(2)–C(3)–Os(1)	126.1(15)

Table 3 (continued)

C(31)–Os(3)–C(3)	89.4(8)	C(2)–C(3)–Os(3)	121.8(13)
C(31)–Os(3)–Os(1)	99.3(7)	Os(1)–C(3)–Os(3)	77.4(6)
C(31)–Os(3)–Os(2)	158.3(6)	C(3)–C(4)–C(5)	125.8(15)
C(32)–Os(3)–C(4)	149.5(6)	C(3)–C(4)–Os(2)	109.8(13)
C(32)–Os(3)–C(3)	147.8(9)	C(3)–C(4)–Os(3)	73.5(10)
C(32)–Os(3)–Os(1)	99.2(7)	C(5)–C(4)–Os(2)	124.2(12)
C(32)–Os(3)–Os(2)	99.7(5)	C(5)–C(4)–Os(3)	120.5(12)
C(4)–Os(3)–Os(1)	70.1(5)	Os(2)–C(4)–Os(3)	77.6(5)
C(4)–Os(3)–Os(2)	49.9(4)	C(4)–C(5)–C(6)	110.0(17)
C(3)–Os(3)–Os(1)	48.9(5)		

[a] Numbers in parentheses are estimated standard deviations in the least significant digit.

B. Solid state structure and VT-NMR of $Os_3(CO)_9(\mu_3\text{-}\eta^2\text{-}CH_3CH_2C{\equiv}CCH_2CH_3)(\mu\text{-}CO)$ (I)

The solid state structure of $Os_3(CO)_9(\mu_3\text{-}\eta^2\text{-}CH_3CH_2C{\equiv}CCH_2CH_2CH_3)(\mu\text{-}CO)$ (I) is illustrated in Fig. 1. Selected bond distances and angles are given in Table 3. The three Os atoms form an isosceles triangle with the longer metal–metal (Os(1)–Os(2)) bond between the osmium atoms which are formally σ bound to the acetylene moiety. These Os atoms are bridged by a carbonyl ligand. The alkyne is coordinated to the cluster with two very similar bonds Os(1)–C(3) (2.13(2) Å), Os(2)-C(4) (2.16(2) Å) and a longer π-bond to the Os(3) atom (2.28(2) Å and 2.24(2) Å). The C(3)–C(4) bond is parallel to the Os(1)–Os(2) edge. On the same side of the triosmium plane is the bridging carbonyl with M–C distances of 2.30(2) and 2.09(2)

Table 4

Low temperature limiting ^{13}C NMR data for $Os_3(CO)_9(\mu_3\text{-}\eta^2\text{-alkyne})L$ complexes, (L = μ-CO, PR_3) [a]

Compound	Terminal carbonyls on			μ-CO/ semibridging CO
	Os(1)	Os(2)	Os(3)	
$Os_3(CO)_9(\mu_3\text{-}\eta^2 - C_2(CH_3CH_2)_2)(\mu\text{-}CO)$ (I)	180.7(2,a) 174.4(2,r) 176.4(2,r)	[b]	180.9(1,a) 175.1(2,r)	193.1(1)
$Os_3(CO)_9(\mu_3\text{-}\eta^2\text{-}C_2(CH_3)_2)(\mu\text{-}CO)$ (II)	180.5(2,a) 177.5(2,r) 176.9(2,r)	[b]	179.9(1,a) 177.3(2,r)	211(1)
$Os_3(CO)_9(\mu_3\text{-}\eta^2\text{-}C_2(CH_3CH_2)_2)(PPh_3)$ (III)	178.8(1,a) 171.8(1,r) 167.2(1,r)	169.0(1,r)	179.2(1,a) 176.0(1,r) 170.8(1,r)	178.2(1) 178.0(1) (^2J(P–C) 9 Hz)
$Os_3(CO)_9(\mu_3\text{-}\eta^2\text{-}C_2(CH_3CH_2)_2)(P(CH_3)_3)$ (IV)	183.2(1,a) 175.7(1,r) 173.0(1,r)	174.8(1,r)	186.3(1,a) 184.4(1,r) 176.5(1,r)	182.7(1) (^2J(P–C) 9 Hz) 180.2(1) (^2J(P–C) 9 Hz)
$Os_3(CO)_9(\mu_3\text{-}\eta^2\text{-}C_2(CH_3)_2)(P(OCH_3)_3)$ (V)	183.2(1,a) 181.7(1,r) 173.7(1,r)	173.3(1,r)	180.9(1,a) 177.2(1,r) 175.3(1,r)	206.2(1) (^2J(P–C) 10 Hz) 181.3(1) (^2J(P–C) 6.6 Hz)

[a] Shifts reported downfield from TMS in CD_2Cl_2; numbers in brackets are relative intensity; r, radial; a, axial disposition. [b] These carbonyls are equivalent to those on Os(1) by symmetry.

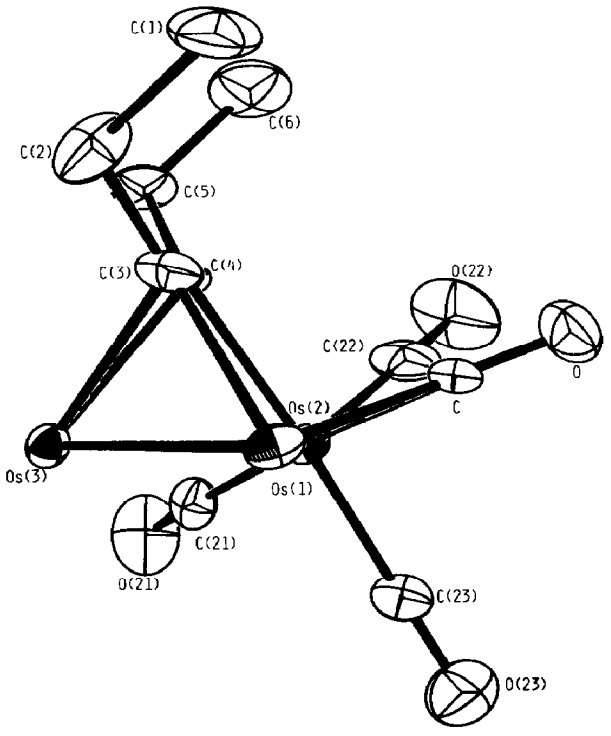

Fig. 2. A view down the Os(1)–Os(2) bond of $Os_3(CO)_{10}((CH_3CH_2)_2C_2)$ (I) showing the geometry around Os(2).

Å (see Fig. 2). If one neglects the Os(1)–Os(2) bond on the doubly bridged edge the Os(1) and Os(2) geometries are almost perfectly octahedral. Thus since the capping alkyne carbons which replace two axial carbonyl groups [in $Os_3(CO)_{12}$] are displaced towards Os(3) the carbonyl groups around Os(1) and Os(2) including the bridging CO are displaced to preserve the octahedral geometry. The asymmetry of this carbonyl bridge is considerably less than that found in the phenyl analog of I where the corresponding M–C distances are 2.76(1) and 1.94(1) Å, respectively.

The 80 MHz ^{1}H NMR spectra of I at $-65\,^\circ$C shows three signals at 2.76 (2, m), 2.17 (2, m), and 1.61 ppm (6, t). The signals are characteristic of two equivalent ABX_3 systems with $^2J_{AB} = 14.1$ Hz and $^2J_{AX} = {}^2J_{BX} = 6.9$ Hz as expected from the solid state structure where the methylene protons are diastereotopic. When the temperature is increased the multiplets at 2.76 and 2.17 ppm due to the CH_2 protons broaden and collapse to a quartet at $+82\,^\circ$C (Fig. 3a). This averaging process can only be obtained by free motion of the alkyne ligand over the face of the metal cluster. Simulation of the ^{1}H NMR spectra gave a set of rate constants (Fig. 3b) which were used to calculate an activation energy for this process of 60.4 ± 2 kJ mol^{-1}.

In order to elucidate whether or not the carbonyl motion is related to the alkyne motion we measured the VT-^{13}C NMR spectra of a ^{13}CO enriched sample of I (Fig. 4). The low temperature limiting ^{13}C NMR spectrum at $-97\,^\circ$C in CD_2Cl_2 is fully consistent with the solid state structure and shows six resonances in the expected relative intensity (Table 4). The downfield resonance at 193.1 ppm is attributed to the bridging carbonyl on the basis of its low field chemical shift and relative

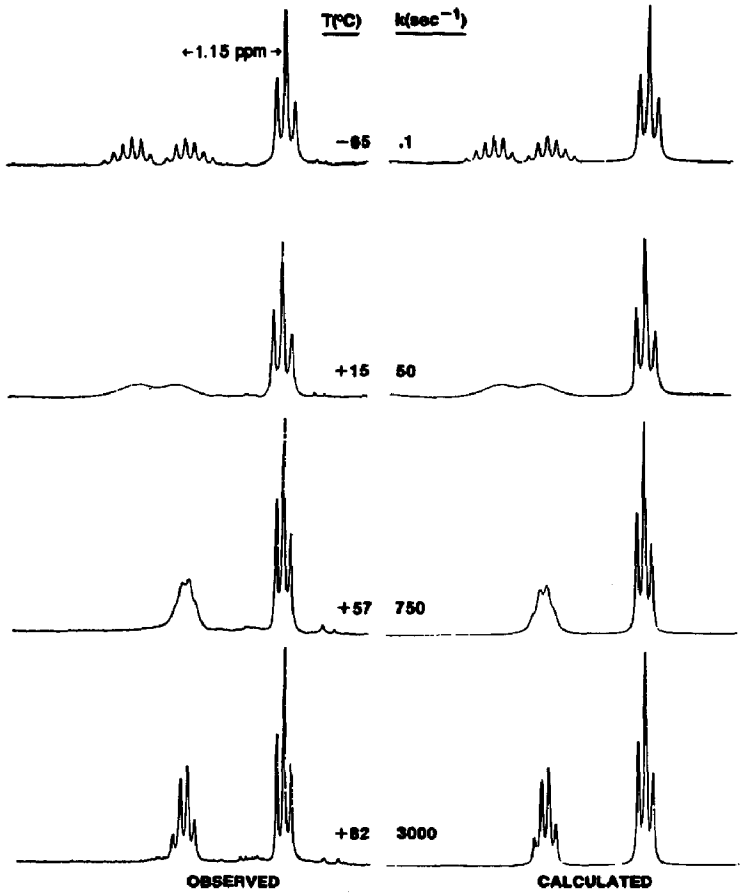

Fig. 3. Observed and calculated ^1H NMR spectra of I from -65 to $+87°C$ in CD_2Cl_2 (-65 to $+30°C$) and C_6D_6 ($+30$ to $+87°C$) at 80 MHz.

intensity. The signals at 180.7, 176.4, and 174.4 ppm are due to the terminal carbonyls bound to Os(1) and Os(2) and the resonances at 180.9 and 175.1 ppm are respectively, the axial and the equatorial carbonyls bound to Os(3). These assignments are made on the basis of their averaging patterns and relative intensity (vide infra). The lowest energy exchange process involves averaging of the resonances which are in a 2/2/2 ratio. This process must be a localised axial–radial exchange of the CO's bound to Os(1) and Os(2) and does not involve the bridging carbonyl. We have estimated the activation energy of this process to be 52.5 ± 2 kJ mol^{-1} by simulating the observed spectra from -97 to $-60°C$. At $-32°C$ the bridging carbonyl resonance broadens and averages with the signal at 177.2 ppm (rel. int. 6) which is the average of the terminal carbonyls on Os(1) and Os(2). At $-20°C$ the signals at 180.9 and 175.1 ppm assignable to the axial and radial carbonyls on Os(3) begin to broaden and all the resonances merge to give a single signal at 177.7 ppm. The activation energy for the process which averages the bridging carbonyl with the terminal carbonyls on Os(1) and Os(2) is estimated to be 60.8 ± 4 kJ mol^{-1} [9*], practically the same value found for averaging of the CH_2 protons in I by ^1H NMR.

* Reference numbers with asterisks indicate notes in the list of references.

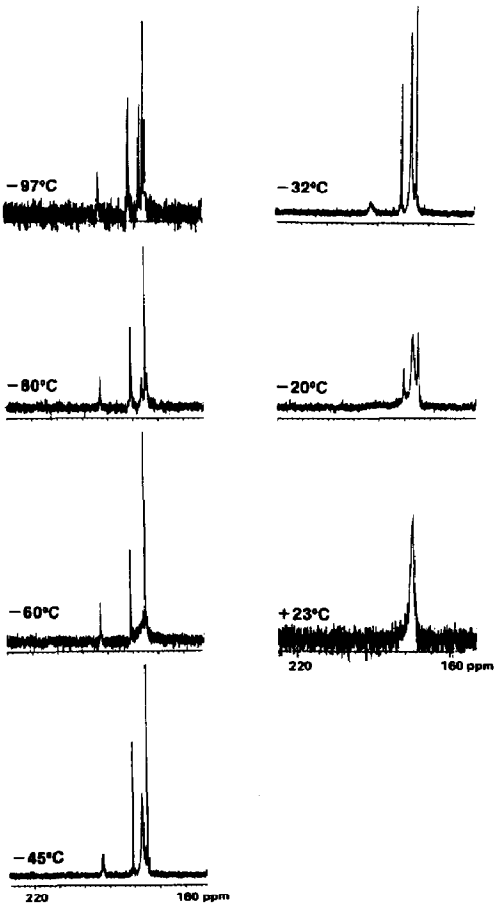

Fig. 4. VT-^{13}C NMR of I from −92 to +30 °C in CD_2Cl_2 at 67.8 MHz.

C, VT-^{13}C-NMR of $Os_3(CO)_9(\mu_3\text{-}\eta^2\text{-}CH_3C{\equiv}CCH_3)(\mu\text{-}CO)$ (II)

In order to evaluate the sensitivity of the observed exchange processes to minor changes in the nature of the R group on the alkyne we examined the VT-^{13}C NMR of $Os_3(CO)_9(\mu_3\text{-}\eta^2\text{-}CH_3C{\equiv}CCH_3)(\mu\text{-}CO)$ (II). The VT-^{13}C NMR of II (Table 4) shows the same processes of carbonyl scrambling with very similar activation energies. The first stage of the exchange involving the terminal carbonyls on Os(1) and Os(2) has an activation free energy of 53.3 ± 4 kJ mol^{-1}. The activation energy for the process which averages the bridging carbonyl with the averaged resonance of the terminal carbonyls on Os(1) and Os(2) is 61.3 ± 4 kJ mol^{-1} [9*]. It was not possible to estimate the activation energy of the axial–radial exchange at Os(3) in either I or II due to overlap of resonances. It is interesting to note that the chemical shift of the bridging carbonyl in I (193 ppm) is 18 ppm to higher field than the same resonance in II (211 ppm) and represents the only significant difference between the VT-^{13}C NMR of I and II. This could be due to the steric properties of the alkyl groups on the alkyne. Furthermore, it should be noted that the chemical shift of the bridging carbonyl is highly temperature dependent below the temperature at which it starts to exchange on the nmr time scale. In estimating the ΔG for the process involving the bridging carbonyl we used the value of its chemical shift at the

temperature at which we observed the onset of exchange on the nmr time scale ($-45\,^{\circ}C$ in II and $-32\,^{\circ}C$ in I). The decrease in the chemical shift of the bridging carbonyl with increasing temperature is consistent with an increasing oscillation of the bridge which averages in an increasing amount of terminal character into the observed chemical shift. We have no firm explanation for the large difference in the chemical shift of the bridging carbonyl in I versus II at this time, as the infrared stretching frequencies of the bridging carbonyls in I and II are virtually the same (Table 2). However, since the carbonyl group is located on the same side of the triangle as the alkyne, there may be a sizeable steric perturbation of the bridging carbonyl chemical shift. The disposition of this carbonyl group also explains why the barrier to axial radial exchange at the doubly bridged edge of the metal triangle is considerably lower than on other doubly bridged cluster edges where the bridging

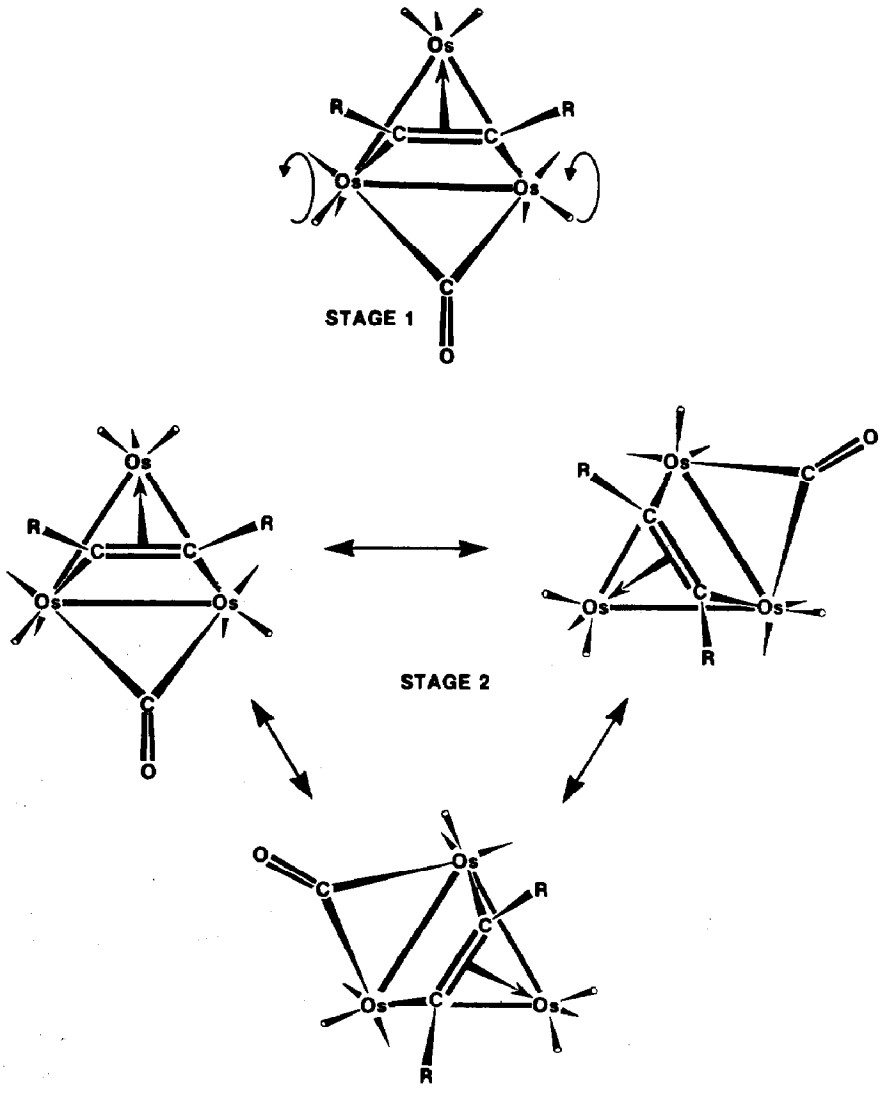

Scheme 1

ligands are on opposite sides of the Os_3 triangle. The fact that the bridging carbonyl is tilted to the same face of the cluster as the alkyne allows the terminal carbonyls to undergo a trigonal twist at a relatively low energy compared with cases where two ligands bridging a common edge but are tilted towards opposite faces of an M_3 triangle [4].

The close similarity in the barriers for averaging of the CH_2 protons in I (60.8 kJ mol^{-1}) to the averaging of the bridge and terminal carbonyls in I and II (60.4 and 61.2 kJ mol^{-1}) suggests that these processes are coupled. The overall process involves simultaneous edge to edge migration of the alkyne and bridging carbonyl (Scheme 1). Coupled with axial–radial exchange at all three osmium atoms this process averages all carbonyl groups and the CH_2 protons of the alkyne. From the data it appears that the onset of axial–radial exchange at Os(3) overlaps with the onset of alkyne migration. We cannot exclude the possibility that bridge-terminal carbonyl exchange at the Os(1)–Os(2) edge precedes the more generalized exchange from these data.

D. Solid state structure of III and VT-NMR of $Os_3(CO)_9(\mu_3\text{-}\eta^2\text{-}(CH_3CH_2)_2C_2)(PR_3)$ *(III–V)*

The reaction of $Os_3(CO)_{10}(\mu_3\text{-}\eta^2\text{-}C_6H_5C{\equiv}CC_6H_5)$ with triphenylphosphine was previously reported to give a monosubstituted derivative $Os_3(CO)_9(\mu_3\text{-}\eta^2\text{-}C_6H_5C{\equiv}CC_6H_5)(P(C_6H_5)_3)$, but no account of the structure was presented [10]. The solid state structure of $Os_3(CO)_9(\mu_3\text{-}\eta^2\text{-}CH_3CH_2C{\equiv}CCH_2CH_3)(P(C_6H_5)_3)$ (III) is shown in Fig. 5 along with selected bond distances and angles given in Table 5. The phosphine substitutes at one of the osmium atoms σ-bonded to the alkyne. Substitution on metal atoms σ-bonded to organic ligands has been observed to be the preferred site in homonuclear trimetallic clusters [2,11]. The primary changes in the structure on comparing I and II are: (1) elongation of the Os–Os bonds at the substituted metal atom (2.832(1), 2.763(1) Å in I and 2.890(1), 2.847(1) Å in III); (2) a pronounced increase in the asymmetry of the bridging carbonyl–metal bonds (Os–CO 2.09(2), 2.30(2) Å in I and 1.94(1), 2.92(1) Å in III); (3) a slight twisting of the alkyne away from the phosphine substituted Os atom [12*]. Indeed the structure of III is almost identical to the $Os_3(CO)_{10}(\mu_3\text{-}\eta^2\text{-}C_6H_5C{\equiv}CC_6H_5)$ structure with respect to the orientation of the alkyne and the asymmetry of the carbonyl bridge (Os–CO 1.94(1), 2.76(1) Å [8]. In addition a second semi-bridging carbonyl is formed upon phosphine substitution involving Os(2)–CO(22)...Os(3) (1.93(1), 2.79(1) Å). Here again this exactly parallels the structure of $Os_3(CO)_{10}(\mu_3\text{-}\eta^2\text{-}C_6H_5C{\equiv}CC_6H_5)$ [8]. The observed twisting of the organic ligand and the increased asymmetry in the bridging carbonyl (CO(21)) can be understood simply in terms of the observed changes in the metal–metal bonds. It is well known that phosphine substitution on clusters causes elongation of the metal–metal bond involving the substituted metal atom [13]. This causes an elongation in one of the Os–C σ bonds (2.16(2) Å, in I, 2.21(1) Å, in III) which in turn causes a compensatory shortening of the other Os–C σ bond (2.13(2) Å in I, 2.09(1) Å in III). These structural changes result in the apparent twist of the organic ligand in III. In suggesting here that the structural changes in III relative to I arise from changes in metal bond lengths only, we cannot assume that this is the case when comparing I with its diphenylacetylene analog. Since diphenylacetylene is considered to be a poorer donor than alkylacetylenes the structure of $Os_3(CO)_{10}(\mu_3\text{-}\eta^2\text{-}C_6H_5C{\equiv}CC_6H_5)$ is probably a consequence

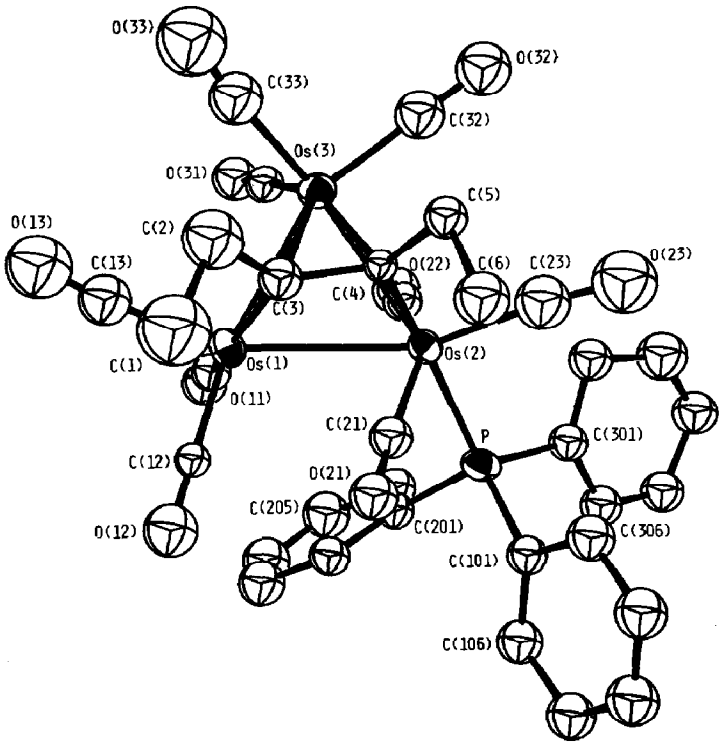

Fig. 5. Perspective view of $Os_3(CO)_9((CH_3CH_2)_2C_2)(P(C_6H_5)_3)$ (III). Thermal ellipsoids represent 50% probability. The numbering of the phenyl ring carbon atoms are numbered sequentially between those labeled.

of the large difference in the steric requirements of diphenyl-versus diethyl-acetylene. There is also considerable distortion in the disposition of the three carbonyl groups on Os(3) in III compared with I. The axial carbonyl, CO(31), in III is displaced toward the Os(1)–Os(3) edge probably in response to the semi-bridging interaction on the Os(2)–Os(3) edge with CO(22). This in turn causes a concomitant displacement of CO(33) in III. All the structural changes observed for III compared with I could be due to the steric demands of the phosphine ligand.

The structural changes observed on going from I to III lead to significant and perhaps, predictable changes in the ligand dynamics of III and related derivatives when compared with I. The ^1H NMR spectra of III at the low temperature limit ($-25\,^\circ C$) is rather complex but a detailed analysis with selective decoupling experiments at different temperatures allows us to assign the spectrum and extract information about the motion of the organic ligand (Fig. 6). At $-25\,^\circ C$ six different signals are observed and the spectrum is interpretable on the basis of two different ABX_3 sets that arise from the asymmetry induced by the phosphine ligand. Furthermore, the most downfield signal (3.09 ppm) shows a small coupling of 3.0 Hz with the phosphorus atom. On increasing the temperature the methylene resonances at 3.09 and 2.89 ppm average and the methylene resonances at 3.02 and 2.44 ppm average. At $+50\,^\circ C$ they collapse into two different broad peaks at 3.06 ppm and 2.64 ppm respectively. At $+65\,^\circ C$, a second stage of exchange is observed and these two signals begin to broaden again, however, decomposition did not allow

Table 5

Interatomic distances (Å) and angles (deg) in III [a]

Distances			
Os(1)–Os(2)	2.890(1)	C(201)–C(202)	1.393(5)
Os(1)–Os(3)	2.734(1)	C(201)–C(206)	1.420(15)
Os(2)–Os(3)	2.847(1)	C(202)–C(203)	1.412(18)
Os(2)–P	2.393(3)	C(203)–C(204)	1.356(20)
Os(1)–C(13)	1.885(12)	C(204)–C(205)	1.378(20)
Os(1)–C(12)	1.898(11)	C(205)–C(206)	1.470(18)
Os(1)–C(11)	1.939(11)	C(301)–C(306)	1.387(15)
Os(1)–C(21)	2.920(11)	C(301)–C(302)	1.397(14)
Os(1)–C(3)	2.093(10)	C(302)–C(303)	1.430(17)
Os(2)–C(4)	2.205(10)	C(303)–C(304)	1.357(17)
Os(2)–C(23)	1.920(13)	C(304)–C(305)	1.435(16)
Os(2)–C(22)	1.926(10)	C(305)–C(306)	1.384(16)
Os(2)–C(21)	1.945(11)	C(11)–O(11)	1.133(14)
Os(3)–C(33)	1.891(13)	C(12)–O(12)	1.127(15)
Os(3)–C(32)	1.915(12)	C(13)–O(13)	1.142(15)
Os(3)–C(31)	1.950(12)	C(21)–O(21)	1.137(14)
Os(3)–C(22)	2.792(10)	C(22)–O(22)	1.161(14)
Os(3)–C(4)	2.141(9)	C(23)–O(23)	1.129(16)
Os(3)–C(3)	2.295(11)	C(31)–O(31)	1.120(15)
P–C(201)	1.832(10)	C(32)–O(32)	1.148(16)
P–C(301)	1.834(10)	C(33)–O(33)	1.135(17)
P–C(101)	1.839(10)	C(1)–C(2)	1.579(20)
C(101)–C(106)	1.394(15)	C(2)–C(3)	1.518(16)
C(101)–C(102)	1.401(15)	C(3)–C(4)	1.393(15)
C(102)–C(103)	1.409(16)	C(4)–C(5)	1.531(14)
C(103)–C(104)	1.351(17)	C(5)–C(6)	1.565(18)
C(104)–C(105)	1.364(18)		
Angles			
Os(3)–Os(1)–Os(2)	60.76(1)	C(13)–Os(1)–Os(3)	96.1(3)
Os(3)–Os(2)–Os(1)	56.91(1)	C(13)–Os(1)–Os(2)	156.7(3)
Os(1)–Os(3)–Os(2)	62.33(1)	C(12)–Os(1)–C(11)	95.9(4)
C(13)–Os(1)–C(12)	94.6(5)	C(12)–Os(1)–C(3)	103.7(4)
C(13)–Os(1)–C(11)	92.3(5)	C(12)–Os(1)–Os(3)	156.6(3)
C(13)–Os(1)–C(3)	93.9(5)	C(12)–Os(1)–Os(2)	105.8(4)
C(11)–Os(1)–C(3)	104.4(3)	C(32)–Os(3)–Os(2)	94.5(4)
C(11)–Os(1)–Os(3)	104.4(3)	C(31)–Os(3)–C(4)	155.1(4)
C(11)–Os(1)–Os(2)	96.5(3)	C(31)–Os(3)–C(3)	131.7(4)
C(3)–Os(1)–Os(3)	54.9(3)	C(31)–Os(3)–Os(1)	86.7(3)
C(3)–Os(1)–Os(2)	70.8(3)	C(31)–Os(3)–Os(2)	108.7(3)
C(23)–Os(2)–C(22)	101.5(5)	C(4)–Os(3)–Os(1)	72.0(3)
C(23)–Os(2)–C(21)	109.7(5)	C(4)–Os(3)–Os(2)	50.0(3)
C(23)–Os(2)–C(4)	87.8(5)	C(3)–Os(3)–Os(1)	48.2(3)
C(23)–Os(2)–P	91.6(4)	C(3)–Os(3)–Os(2)	69.3(3)
C(23)–Os(2)–Os(3)	103.0(4)	C(201)–P–C(301)	104.1(5)
C(23)–Os(2)–Os(1)	155.1(4)	C(201)–P–C(101)	105.9(4)
C(22)–Os(2)–C(21)	146.7(4)	C(201)–P–Os(2)	112.7(3)
C(22)–Os(2)–C(4)	116.2(4)	C(301)–P–C(101)	102.4(5)
C(22)–Os(2)–P	83.6(3)	C(301)–P–Os(2)	117.4(3)
C(22)–Os(2)–Os(3)	68.5(3)	C(101)–P–Os(2)	113.1(3)
C(22)–Os(2)–Os(1)	85.3(3)	C(106)–C(101)–C(102)	121.0(9)
C(21)–Os(2)–C(4)	77.0(4)	C(101)–C(102)–C(103)	120.0(10)
C(21)–Os(2)–P	84.4(4)	C(104)–C(103)–C(102)	120.2(11)
C(21)–Os(2)–Os(3)	113.6(4)	C(103)–C(104)–C(105)	120.4(12)
C(21)–Os(2)–Os(1)	71.3(3)	C(104)–C(105)–C(106)	122.4(11)

Table 5 (continued)

C(4)–Os(2)–P	159.9(2)	C(101)–C(106)–C(105)	115.9(10)
C(4)–Os(2)–Os(3)	48.1(2)	C(202)–C(201)–C(206)	122.1(10)
C(4)–Os(2)–Os(1)	68.0(3)	C(201)–C(202)–C(203)	119.5(11)
Os(3)–Os(2)–P	150.44(6)	C(204)–C(203)–C(202)	120.2(12)
Os(1)–Os(2)–P	113.06(6)	C(203)–C(204)–C(205)	122.2(13)
C(33)–Os(3)–C(32)	92.6(5)	C(204)–C(205)–C(206)	120.2(12)
C(33)–Os(3)–C(31)	91.6(5)	C(201)–C(206)–C(205)	115.7(10)
C(33)–Os(3)–C(4)	107.2(5)	C(306)–C(301)–C(302)	120.8(10)
C(33)–Os(3)–C(3)	88.5(5)	C(301)–C(302)–C(303)	118.1(10)
C(33)–Os(3)–Os(1)	108.7(4)	C(304)–C(303)–C(302)	122.2(11)
C(33)–Os(3)–Os(2)	156.5(4)	C(303)–C(304)–C(305)	118.2(11)
C(32)–Os(3)–C(31)	102.0(5)	C(306)–C(306)–C(304)	120.7(10)
C(32)–Os(3)–C(4)	93.6(4)	C(305)–C(306)–C(301)	120.1(9)
C(32)–Os(3)–C(3)	126.3(4)	O(11)–C(11)–Os(1)	176.5(10)
C(32)–Os(3)–Os(1)	156.9(4)	O(12)–C(12)–Os(1)	178.3(11)
O(13)–C(13)–Os(1)	177.2(10)	C(2)–C(3)–Os(1)	126.2(8)
O(21)–C(21)–Os(2)	174.6(10)	C(2)–C(3)–Os(3)	122.3(8)
O(22)–C(22)–Os(2)	167.6(9)	Os(1)–C(3)–Os(3)	76.9(3)
O(23)–C(23)–Os(2)	178.9(11)	C(3)–C(4)–C(5)	125.6(10)
O(31)–C(31)–Os(3)	177.7(10)	C(3)–C(4)–Os(3)	77.8(6)
O(32)–C(32)–Os(3)	176.7(12)	C(3)–C(4)–Os(2)	108.4(7)
O(33)–C(33)–Os(3)	177.9(11)	C(5)–C(4)–Os(3)	124.9(7)
C(3)–C(2)–C(1)	108.8(10)	C(5)–C(4)–Os(2)	122.3(7)
C(4)–C(3)–C(2)	122.5(10)	Os(3)–C(4)–Os(2)	81.8(3)
C(4)–C(3)–Os(1)	111.2(7)	C(4)–C(5)–C(6)	111.6(9)
C(4)–C(3)–Os(3)	65.8(6)		

[a] Numbers in parentheses are estimated standard deviations in the least significant digit.

us to determine the coalescence temperature for this higher energy process. The first stage of exchange is estimated to be 66 ± 4 kJ mol^{-1}. The $\Delta G^{\neq}$ for the process which averages the methyl groups is estimated to be 68 ± 4 kJ mol^{-1}. That there are two stages of alkyne motion is evident from the averaging pattern of the methylene protons in III, IV, but the estimate of the second stage exchange process from the averaging of the methyl groups in III must clearly be low due to their small chemical shift difference. The first stage of exchange must average two methylene protons but not the methyl protons. The second stage process averages the two ends of the alkyne. A restricted pivotal motion of the alkyne around the carbon on the phosphine substituted Os(2) coupled with localized phosphine–carbonyl exchange would explain the first exchange process (Scheme 2). The second process of exchange involves free motion of the alkyne over the face of the cluster as for I [14*].

We have also examined the VT-^{1}H NMR of $Os_3(CO)_9(\mu_3\text{-}\eta^2\text{-}CH_3CH_2C{\equiv}CCH_2CH_3)(P(CH_3)_3)$ (IV). The low temperature limiting spectrum of the organic moiety is virtually identical in form with that of III (Table 1). Line shape analysis gave estimated activation free energies very similar to those of III for both stages of the alkyne motion (65 ± 4 kJ mol^{-1} and 67 ± 4 kJ mol^{-1}). It is clear from these results that neither the size nor the donor ability of the phosphine have a significant effect on the mobility of the organic ligand in the substituted derivatives. However, the barrier to alkyne motion is significantly higher in both III and IV when compared with I. This result is somewhat surprising in light of the fact that the Os–alkyne

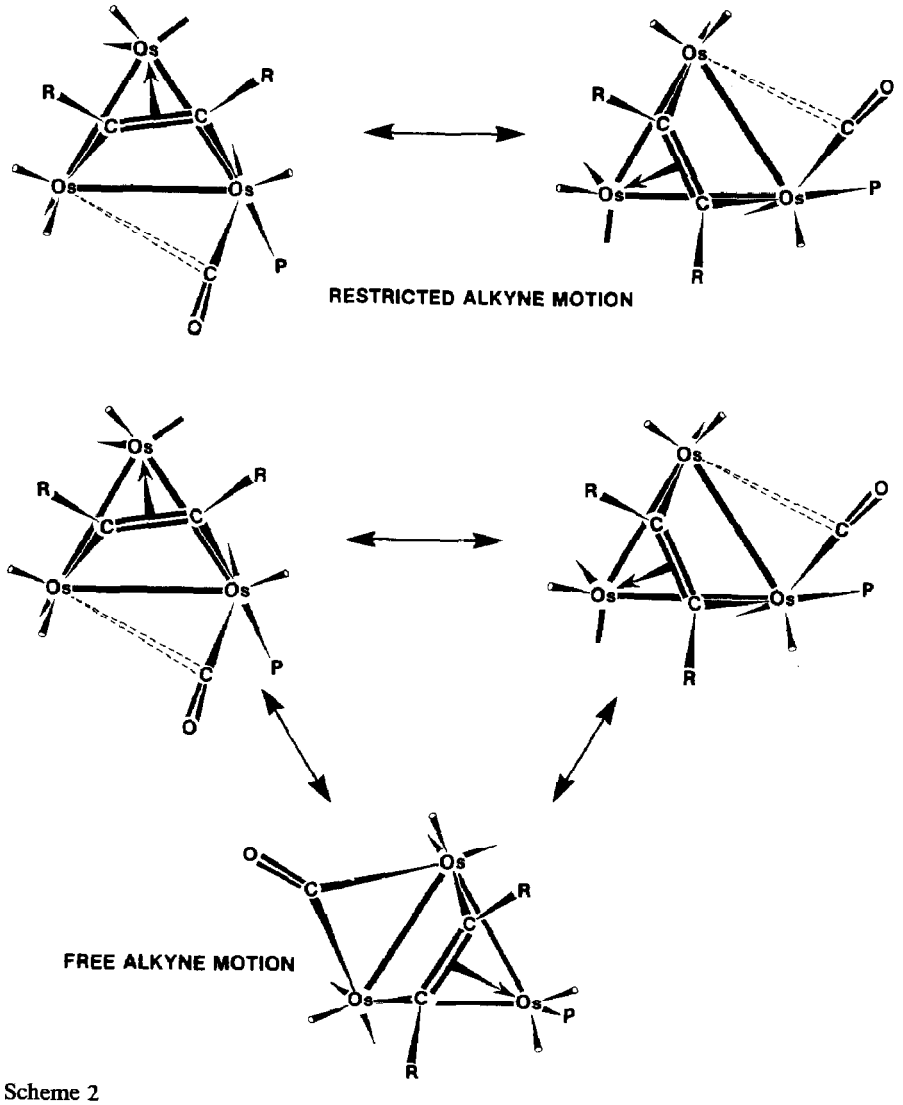

Scheme 2

bonds to the phosphine substituted Os atom are longer in III than the same bonds in I.

The VT-^{1}H NMR of $Os_3(CO)_9(\mu_3\text{-}\eta^2\text{-}CH_3C{\equiv}CCH_3)(P(OCH_3)_3)$ (V) (Table 1) shows two resonances for the methyl groups of the alkyne in the low temperature ($-60\,^\circ$C) spectrum. As the temperature is increased these signals remain sharp until $+40\,^\circ$C where they begin to broaden. Above this temperature decomposition was too rapid to allow evaluation of the activation energy at coalescence. The overall behavior is consistent with the two stage alkyne motion actually observed for III and IV.

The VT-^{13}C NMR (Fig. 7) of V clearly reflects the changes in ground state geometry and the two stage alkyne exchange observed on going from I to III, IV or V. Its ^{13}C NMR spectrum will be discussed before III or IV since the chemical shifts in this complex allow a clearer interpretation of the data. The low temperature

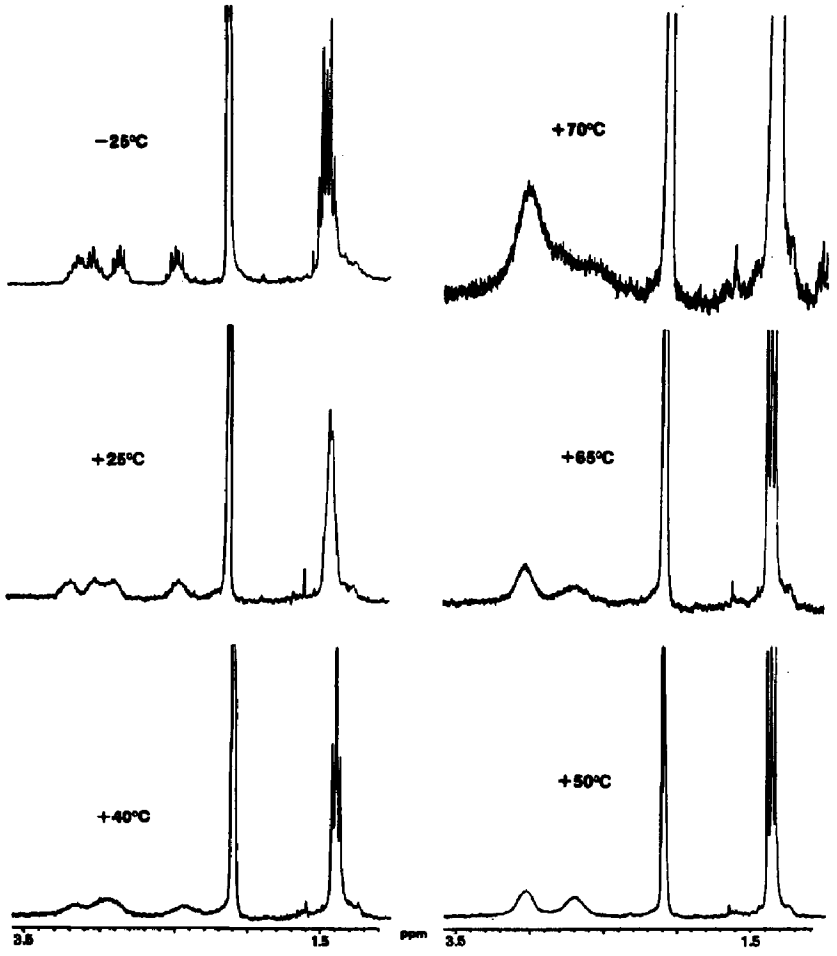

Fig. 6. VT-^{1}H NMR of III from −25 to +50 °C in $CD_3C_6D_5$ at 270 MHz.

limiting spectrum (−62 °C) of V shows the expected nine resonances all with relative intensities of one (Table 4). The resonances can be partially assigned on the basis of their averaging pattern, chemical shift and phosphorus–carbon coupling constants. The resonance at 206.2 ppm is assigned to the semibridging carbonyl on the basis of its downfield chemical shift and measurable two bond carbon–phosphorus coupling constant. The resonances at 181.3 and 173.3 ppm are assigned to the terminal carbonyls on Os(2) on the basis of a measurable phosphorus–carbon coupling to the resonance at 181.3 ppm and the fact that these resonances average with each other and the semibridging carbonyl at higher temperatures. The infrared data for III–V (Table 2) and the solid state structure of III, as well as $Os_3(CO)_{10}(\mu_3\text{-}\eta^2\text{-}C_6H_5C{\equiv}CC_6H_5)$, indicate the presence of two semibridging carbonyls yet the ^{13}C-NMR data for V shows only one carbonyl resonance in the semibridging region. Apparently one of the semibridging carbonyls on Os(2) is shifted into the terminal region. We tentatively assign the more downfield resonance to the semibridging carbonyl on the Os(1)–Os(2) edge since it shows the pronounced sensitivity to changes in alkyl group as the bridging carbonyl in I and II. Indeed in III and IV (vide infra, Table 4) both semibridging carbonyls on Os(2) are

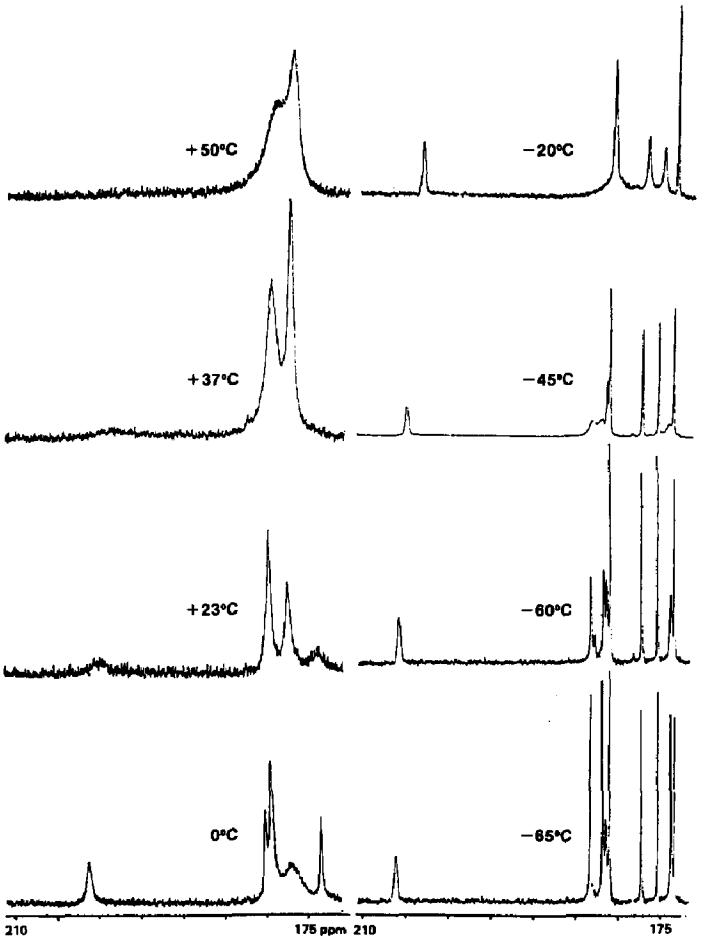

Fig. 7. VT-^{13}C NMR of V at 67.8 MHz in CD_2Cl_2.

observed in the formally terminal region. The resonances at 183.2, 181.7, and 173.7 ppm can be assigned to the carbonyls on Os(1) since they are observed to average with each other at a lower temperature than the remaining three resonances at 180.9, 177.2, and 175.3 ppm. These are assigned to the carbonyls on Os(3) which average with each other at higher temperature. The overall pattern of carbonyl exchange in V is distinctly different from that observed for I or II. The carbonyls on Os(1) average to a single resonance at 179.4 ppm by a localized axial-radial exchange in the temperature range from -62 to $0\,^\circ$C. The carbonyls on Os(3) average to a single resonance at 177.0 ppm in the temperature range from -27 to $+20\,^\circ$C. The terminal carbonyl and the two semibridging carbonyls on Os(2) also independently average in the temperature range from 0 to $50\,^\circ$C. We were able to estimate the activation free energies from independent line shape analysis on each group of resonances. The barriers for localized exchange on Os(1), and Os(3) are very close being 50.2 and 51.8 kJ mol^{-1}. The barrier for the process which averages the two semibridging carbonyls with the terminal carbonyl on Os(2) is estimated to be 58 kJ mol^{-1}. This value was obtained using the chemical shift for the bridging carbonyl of 201.3 ppm (shift at $0\,^\circ$C). The fact that the chemical shift decreases with increasing

temperature naturally makes this estimate low. Taking this data together with those obtained from the VT-^{1}H NMR of III, IV, and V we propose that edge to edge migration of the semibridging carbonyl is coupled to the pivotal motion of the alkyne ligand as depicted in Scheme 2. The activation energy of 58 kJ mol^{-1} for averaging of the semibridging carbonyl in V is somewhat lower than that observed for the methylene protons (66–67 kJ mol^{-1}) in III and IV. This may be due to the large differences in donor ability expected between $P(OR)_3$ and PR_3 ligands or to inaccuracies in the calculations due to the observed temperature dependence of the semibridging CO chemical shift. However, the pivotal motion of the alkyne observed for III, IV, and V must be coupled with edge to edge migration of the semibridging carbonyls or the methylene environments in III and IV would not be averaged (see Scheme 2).

Using a highly enriched sample of IV ($^{13}CO \approx 30$–40%) we examined its VT-^{13}C NMR in the carbonyl region at 67.8 MHz in $CDCl_3$. The low temperature limiting spectrum was reached at $-65\,^\circ$C and showed the expected nine resonances all of equal integrated relative intensity (Table 4). The same three stages of localized exchange can be observed as for V with assignments being aided here by the high level enrichment which was necessary due to the unexpected high field chemical shift of the semibridging carbonyls (Table 4). The final stage of exchange in the ^{13}C NMR of the carbonyl region involving the semibridging carbonyls has approximately the same activation energy as the oscillating motion of the alkyne as determined from the ^{1}H NMR of the methylene groups in IV (66 ± 4 kJ mol^{-1}).

The VT-^{13}C NMR of an ^{13}CO enriched sample of III was also measured. At the low temperature limit nine resonances of equal intensity (Table 4) are observed. As the temperature is increased the same three stages of exchange are observed. Here again as for IV the final stage of exchange involving the semibridging carbonyl is estimated to have an activation energy similar to the oscillatory motion of the alkyne (65 ± 4 kJ mol^{-1}). These results indicate that the localized exchange at the phosphine substituted osmium involving the two semibridging carbonyls is directly coupled to the restricted alkyne motion. At higher temperatures ($> 55\,^\circ$C) free motion of the alkyne can be inferred from the ^{13}C- and ^{1}H NMR data. Finally, it is worth pointing out that the chemical shift of one of the semibridging carbonyls in III and IV is over 20 ppm upfield of that in V. This may be due to the difference in donor abilities of the phosphines (the IR data do not support this) or the steric perturbation by the alkyl group. Recalling the similar difference observed for the bridging CO in I compared with II, steric perturbation by the alkyl group (in solution) seems to be the stronger influence. The semibridging carbonyls could be assigned with certainty in III from the large phosphorous–carbon coupling constant to the resonance at 178.0 ppm and the observed patterns of averaging as for IV.

Experimental

Materials. Dodecacarbonyltriosmium, $Os_3(CO)_{12}$, was purchased from Strem Chemicals and used as received to prepare $H_2Os_3(CO)_{10}$ [15]. $Os_3(CO)_9(\mu_3\text{-}\eta^2\text{-}RC{\equiv}CR)(\mu\text{-}CO)$ ($R = CH_3$, CH_2CH_3) were prepared according to literature procedures [3,7] using $H_2Os_3(CO)_{10}$ and 2-butyne or 3-hexyne purchased from Aldrich. Solvents were ACS reagent grade (methylene chloride, hexane, cyclohexane, and octane obtained from Mallinkrodt) and were stored over molecular sieves. Deu-

terated NMR solvents were purchased from Aldrich and also stored over molecular sieves. Enrichment (15–20%) of $Os_3(CO)_{12}$ with ^{13}CO as accomplished by heating $Os_3(CO)_{12}$ in octane at 110°C for 5 days under 0.5 atm 90% ^{13}C carbon monoxide.

Spectra. Nuclear magnetic resonance spectra were obtained on an IBM-NR/80 (^1H NMR 80 MHz) or a Jeol-GX-270 (^1H NMR 270 MHz, ^{13}C NMR 67.8 MHz) spectrometer operating in the Fourier transform mode. Variable temperature measurements were calibrated against the $\Delta\delta$ values (δ(OH)–δ(CH)) in CH_3OH (−100 to +25°C) and $(CH_2OH)_2$ (+25 to +95°C) samples. Line shape analysis of VT-^1H and -^{13}C NMR spectra were performed using a version of DNMR-4 by Gerhard and Binsch [9*]. Activation free energies, $\Delta G^{\neq}$, were estimated using calculated rate constants obtained from at least five temperatures and the slope of the ln k vs $1/T$ fit to a standard least squares program. Infrared data were obtained on a Nicolet-20D × B spectrometer operating at 1.0 wave number resolution.

Analyses. Elemental analysis was performed by Schwartzkopf Microanalytical Laboratories.

Synthesis of $Os_3(CO)_9(\mu_3\text{-}\eta^2\text{-}RC{\equiv}CR)L$ ($R = CH_3$, CH_2CH_3, $L = P(C_6H_5)_3$, $P(CH_3)_2C_6H_5$, $P(CH_3)_3$, $P(OCH_3)_3$. In a typical procedure 100 mg (0.10 mmol) of

Table 6

Summary of crystallographic data for I and III

Formula	$C_{16}H_{10}O_{10}Os_3$ (I)	$C_{33}H_{25}O_9POs_3$ (III)
FW	932.8_5	1167.1_3
Cryst sys., sp. gr.	triclinic, $P\bar{1}$	monoclinic, $P2_1/c$
a, Å	9.292(2)	14.271(4)
b, Å	5.340(3)	11.370(2)
c, Å	8.391(2)	21.192(5)
α, deg	91.27(2)	
β, deg	116.70(1)	104.43(2)
γ, deg	105.24(2)	
V, Å^2	1017.3(4)	3330(1)
Z	2	4
d_{calcd}, g/cm^3	3.045	2.328
Cryst size, mm	0.26×0.38×0.34	0.25×0.34×0.31
Radiation (λ, Å)	Mo-K_α (0.71069)	Mo-K_α (0.71069)
Abs coeff, μ(cm^{-1})	187.6	115.3
Scan range, deg	$2.5 < 2\theta \leq 46$	$2.5 < 2\theta \leq 50$
Scan speed, deg/min	2.0–19.0 (-2θ)	2.0–19.0 (θ –2θ)
Ratio bkgd/scan time	0.5	0.5
No. of data collcd	3042 ($+h, \pm k, \pm l$)	5899 ($+h, -k, \pm l$)
No. of observns [$F_0^2 > 3\sigma(F_0^2)$]	2659	4512
No. of variables	262	325
R [a]	0.044	0.033
R_w [b]	0.058	0.041
GOF [c]	2.19	1.43
Largest peak, e/Å^3	1.04	0.98
Largest Δ/σ, final cycle	0.01	0.10

[a] $R = \Sigma||F_0| - |F_c||/\Sigma|F_0|$. [b] $R_w = [\Sigma w(|F_0| - |F_c|)^2/\Sigma w|F_0|^2]^{1/2}$. [c] $GOF = [\Sigma w(|F_0| - |F_c|)^2/(N_{observns} - N_{parameters})]^{1/2}$.

$Os_3(CO)_9(\mu_3\text{-}\eta^2\text{-}RC{\equiv}CR)(\mu\text{-}CO)$ was dissolved in 100 ml of cyclohexane under nitrogen. One equivalent of the appropriate phosphine or phosphite was added by syringe or as a solid [$P(C_6H_5)_3$] and the reaction refluxed for 3–4 h under nitrogen. At this time almost all of the starting material was consumed and only one product was formed as monitored by analytical TLC (silica gel, hexane eluent). The solution was then rotary evaporated to dryness. The residue was taken up in a minimum amount of CH_2Cl_2 and the product purified by preparative TLC (Silica Gel PF-254, 10% CH_2Cl_2/hexanes as eluent). A single product band was isolated and recrystallized from hexanes at −20 °C. Typical yields ranged from 65–75% (see Tables 1–3 for spectroscopic and analytical data).

X-ray data and structure solution. Crystals of I (red) and III (yellow) obtained from hexane solutions were mounted in air on the tip of small glass fibers in a random orientation. The crystal lattices of I and III were determined from the auto-indexing routine of the Data General/Nova diffractometer software and axial photographs. Final lattice parameters, calculated, from the refined settings of 15

Table 7

Final positional and thermal parameters with their standard deviations in parentheses for I [a]

Atom	x	y	z	B (Å^2)
Os(1)	0.79544(8)	0.28760(4)	0.77762(8)	1.93(2)
Os(2)	0.44986(8)	0.27584(4)	0.57301(8)	1.71(2)
Os(3)	0.61054(8)	0.31160(4)	0.94635(8)	1.85(2)
C	0.5881(23)	0.2159(11)	0.4915(23)	2.7(6)
O	0.5827(17)	0.1744(8)	0.3750(17)	3.8(5)
C(11)	0.8750(22)	0.3964(13)	0.7046(24)	3.3(6)
O(11)	0.9242(21)	0.4698(11)	0.6623(23)	6.5(7)
C(12)	0.9091(22)	0.2217(14)	0.7042(26)	3.4(6)
O(12)	0.9733(18)	0.1810(11)	0.6604(22)	5.8(6)
C(13)	0.9798(22)	0.3289(13)	1.0131(25)	2.9(6)
O(13)	1.0932(17)	0.3487(11)	1.1519(19)	4.6(5)
C(21)	0.3171(22)	0.3335(12)	0.6361(21)	2.6(6)
O(21)	0.2260(18)	0.3661(11)	0.6522(19)	5.6(6)
C(22)	0.2547(26)	0.1957(12)	0.3697(25)	3.6(7)
O(22)	0.1366(20)	0.1480(11)	0.2530(19)	5.7(6)
C(23)	0.4928(21)	0.3739(12)	0.4501(22)	2.4(6)
O(23)	0.5222(21)	0.4341(10)	0.3751(19)	5.5(6)
C(31)	0.7643(23)	0.3083(12)	1.1858(24)	3.0(6)
O(31)	0.8629(18)	0.3091(12)	1.3304(19)	5.4(6)
C(32)	0.6726(24)	0.4428(14)	0.9829(23)	3.3(7)
O(32)	0.7026(20)	0.5190(9)	0.9967(19)	4.9(6)
C(33)	0.4327(22)	0.2876(11)	1.0043(22)	2.4(6)
O(33)	0.3205(17)	0.2739(10)	1.0350(18)	4.4(5)
C(1)	0.7515(30)	0.0443(13)	0.8850(31)	5.6(9)
C(2)	0.7126(24)	0.1183(14)	0.9801(26)	4.0(7)
C(3)	0.6484(22)	0.1828(11)	0.8531(23)	2.8(6)
C(4)	0.4800(20)	0.1775(10)	0.7573(20)	1.9(5)
C(5)	0.3310(23)	0.1058(11)	0.7639(25)	3.2(6)
C(6)	0.2661(29)	0.0187(14)	0.6222(32)	5.3(9)

[a] Anisotropically refined atoms are given in the form of the isotropic equivalent B defined as $(4/3)[a^2B_{11} + b^2B_{22} + c^2B_{33} + ab(\cos\gamma)B_{12} + ac(\cos\beta)B_{13} + bc(\cos\alpha)B_{23}]$.

Table 8

Final positional and thermal parameters with their standard deviations in parentheses for III [a]

Atom	x	y	z	B (Å^2)
Os(1)	0.09386(3)	0.16004(3)	0.62753(2)	2.43(1)
Os(2)	0.26580(3)	0.30426(3)	0.65050(2)	2.22(1)
Os(3)	0.15608(3)	0.27250(4)	0.74451(2)	2.66(1)
P	0.3820(2)	0.2343(2)	0.5952(1)	2.20(6)
C(11)	0.1600(8)	0.0097(10)	0.6404(5)	3.3(3)
O(11)	0.1977(6)	−0.0784(7)	0.6509(4)	4.7(2)
C(12)	0.0489(8)	0.1470(9)	0.4813(4)	6.6(3)
O(12)	0.0202(8)	0.1380(8)	0.4813(4)	6.6(3)
C(13)	−0.0190(8)	0.0957(10)	0.6447(6)	3.8(3)
O(13)	−0.0874(6)	0.0603(9)	0.6568(5)	6.3(3)
C(21)	0.1870(8)	0.3358(9)	0.5632(6)	3.4(3)
O(21)	0.1461(6)	0.3609(7)	0.5117(4)	4.1(2)
C(22)	0.3228(7)	0.1868(9)	0.7140(5)	2.9(3)
O(22)	0.3659(6)	0.1101(8)	0.7439(4)	4.8(2)
C(23)	0.3440(10)	0.4393(11)	0.6827(6)	4.8(4)
O(23)	0.3893(7)	0.5196(8)	0.7007(5)	6.8(3)
C(31)	0.1837(7)	0.1168(10)	0.7833(5)	3.3(3)
O(31)	0.1977(6)	0.0259(8)	0.8037(4)	5.0(3)
C(32)	0.2378(9)	0.3708(10)	0.8087(6)	4.2(3)
O(32)	0.2905(7)	0.4275(8)	0.8463(5)	6.1(3)
C(33)	0.0498(9)	0.2916(11)	0.7819(6)	4.4(4)
O(33)	−0.0159(7)	0.3023(10)	0.8025(5)	7.3(4)
C(1)	−0.0979(10)	0.3844(16)	0.5662(7)	7.1(5)
C(2)	−0.0426(8)	0.3807(11)	0.6406(6)	4.6(4)
C(3)	0.0585(8)	0.3328(9)	0.6467(5)	3.3(3)
C(4)	0.1413(7)	0.4010(8)	0.6688(4)	2.6(2)
C(5)	0.1430(9)	0.5343(9)	0.6793(6)	4.2(3)
C(6)	0.1346(12)	0.6026(10)	0.6141(7)	5.9(5)
C(101)	0.3811(7)	0.3178(9)	0.5207(5)	2.6(2)
C(102)	0.3709(8)	0.4402(10)	0.5221(5)	3.4(2)
C(103)	0.3768(9)	0.5083(11)	0.4677(6)	4.3(2)
C(104)	0.3934(9)	0.4560(11)	0.4143(6)	4.4(2)
C(105)	0.4025(9)	0.3367(11)	0.4119(6)	4.3(2)
C(106)	0.3974(8)	0.2613(10)	0.4660(5)	3.7(2)
C(201)	0.3622(7)	0.0804(9)	0.5697(5)	2.7(2)
C(202)	0.2815(8)	0.0526(10)	0.5198(5)	3.8(2)
C(203)	0.2589(10)	−0.0665(12)	0.5042(6)	5.1(3)
C(204)	0.3137(10)	−0.1532(12)	0.5390(7)	5.2(3)
C(205)	0.3940(10)	−0.1297(12)	0.5889(7)	5.5(3)
C(206)	0.4208(8)	−0.0076(10)	0.6079(5)	3.9(2)
C(301)	0.5099(7)	0.2396(8)	0.6395(5)	2.6(2)
C(302)	0.5365(8)	0.2811(9)	0.7036(5)	3.4(2)
C(303)	0.6374(9)	0.2899(11)	0.7347(6)	4.2(2)
C(304)	0.7068(8)	0.2588(10)	0.7042(5)	3.7(2)
C(305)	0.6767(8)	0.2156(10)	0.6386(5)	3.8(2)
C(306)	0.5795(7)	0.2070(9)	0.6074(5)	3.0(2)

[a] Anisotropically refined atoms are given in the form of the isotropic equivalent B defined as $(4/3)[a^2B_{11} + b^2B_{22} + c^2B_{33} + ac(\cos\beta)B_{13}]$.

reflections ($14° < 2\theta < 26°$) on a Nicolet/Syntex $P2_1$ diffractometer, are given in Table 6. Intensity data were collected by the θ–2θ scan technique at room temperature ($24 \pm 2°$ C). Three standard reflections were monitored after every 100 reflections measured. The variation in their intensities was within 3% over time required for data acquisition. The data were merged ($R_{int} = 0.043$, $0k0$; $00l$ (II), and $R_{int} = 0.027$ (III)), and corrected for Lorentz and polarization effects [16*]. An absorption correction was applied using the empirical ψ-scan method.

Solution and refinement of structures. The position of the three osmium atoms in I were determined from a Patterson map. The structure of III was solved by direct methods [17]. A subsequent structure factor difference Fourier map calculated using the phases of the osmium atoms and phosphorus(III) revealed the position of all other nonhydrogen atoms in the metal clusters. The structures were first refined isotropically by full matrix least squares [18*]. In the final cycles of refinement anisotropic thermal parameters were assigned to all nonhydrogen atoms, with the exception of the phenyl carbons in III. The function minimized during refinement was $\sum w(|F_0| - |F_c|)^2$ where the weights were calculated according to the expression $w = 4F_0^2/\sigma^2(F_0^2)$. The final agreement factors and refinement parameters are given in Table 6. Refined positional and thermal parameters for I and III are listed in Tables 7 and 8. Hydrogen atoms were not located in any of the structures. Atomic scattering factors for Os, P, O, C, and H were used and the osmium atoms were corrected for anomalous dispersion [19]. Atomic parameters and tables of observed and calculate structure factors are available.

Supplementary materials available. Listings of structure factor amplitudes, final positional and anisotropic thermal parameters. Ordering information is given on any current masthead page.

Acknowledgements

We gratefully acknowledge the National Foundation (CHE-8711549) and the donors of the Petroleum Research Foundation administered by the American Chemical Society (19781-B3-C) for support of this research. We also thank the Computer Center of the California State University, Los Angeles for providing time on the CDC Cyber 760 and the CNR of Italy for a Nato fellowship (RG).

References and footnotes

1 (a) K. Burgess, Polyhedron, 3 (1984) 1175.
(b) B.F.G. Johnson, Transition Metal Clusters, J. Wiley and Sons Ltd, Chichester, 1980.
2 S. Aime, R. Gobetto, D. Osella, L. Milone, and E. Rosenberg, Organometallics, 1 (1983) 640.
3 E. Rosenberg, E.V. Anslyn, C.B. Thorsen, S. Aime, D. Osella, R. Gobetto, and L. Milone, Organometallics, 3 (1984) 1790 and ref. therein.
4 S. Aime, O. Gambino, L. Milone, E. Sappa and E. Rosenberg, Inorg. Chim. Acta, 15 (1975) 53.
5 C.B. Thorsen, E. Rosenberg, G. Saatjian, S. Aime, L. Milone and D. Osella, Inorg. Chem., 20 (1981) 1592.
6 B.F.G. Johnson, J. Lewis and K.T. Schorpp, J. Organomet. Chem., 91 (1975) C13.
7 A.J. Deeming, S. Hasso and M. Underhill, J. Chem. Soc. (Dalton), (1975) 1614.
8 C.G. Pierpont, Inorg. Chem., 16 (1977) 636.
9 This value was estimated using an approximate line shape program (POLY), S.O. Chan and L.W. Reeves, J. Am. Chem. Soc., 95 (1973) 673, since the number of spins was too great to use the more accurate DNMR-4 program, D.A. Klier, and G. Binsch, J. Magn. Res., 3 (1970) 146.

10 J.R. Shapley, M. Tachikawa, C.G. Pierpont, J. Am. Chem. Soc., 97 (1975) 7172.
11 C. Jangala, E. Rosenberg, D. Skinner, S. Aime, L. Milone and E. Sappa, Inorg. Chem., 19 (1980) 1671.
12 We have obtained the solid state structure of the dimethylphenylphosphine derivative of I. $Os_3(CO)_9(\mu_3\text{-}\eta^2\text{-}CH_3CH_2C{\equiv}CCH_2CH_3)P(CH_3)_2C_6H_5$ (VI), which we will report separately. The structure of this complex is virtually identical to III. Crystal data: crystals of VI are triclinic, space group $P\bar{1}$, with a 9.671(3) Å, b 16.231(5) Å, c 9.049(2) Å, α 91.92(2)°, β 97.13(2)°, γ 106.99(2)°, V 1344.3(6) Å^3, and $Z = 2$. Final agreement factors for 3957 observations, $I > 3\sigma(I)$, are $R_F = 0.032$, $R_{wF} = 0.043$, and GOF = 1.63.
13 R.D. Adams and J.P. Selegue, Abstr. Am. Cryst. Soc., August, 1980 p. 28.
14 We have also considered a two edge swivel motion which would average the ends of the alkyne during first stage of exchange but leave the methylenes protons on individual carbons diastereotopic. The ^1H NMR data for V shows that is not the case.
15 A.J. Deeming and S. Hasso, J. Organomet. Chem., 88 (1975) C21.
16 The net integrated intensity, I, and its estimated standard deviation, $\sigma(I)$, were calculated from the equations: $I = R^*[C - t(B_1 + B_2)]$, $\sigma(I) = [R^*(C + t^2(B_1 + B_2) + (pI)^2]^{1/2}$, $F_0^2 = 1\{^*\text{Abs}^*\text{I}$, and $\sigma(F_0^2) = \text{Lp}^*\text{Abs}^*\sigma(\text{I})$. Here R is the scan rate, t is the ratio of intensity scan time to time of background count, p, the "ignorance factor" was set equal to 0.04, Abs is an empirical absorption correction, and Lp is the Lorentz and polarization factor. The Lorentz and polarization correction is from Churchill, et. al., Inorganic Chem., 16 (1977) 265, and used to give F_0^2 and $\sigma(F_0^2)$.
17 MULTAN: A system of computer programs for the automatic solution of crystal structures from X-ray diffraction data, Germain, G., Main, P., Woolfson, M.M., Acta, Cryst. A, 27 (1971) 368.
18 Programs used include a modified version of Bushing and Levy group least squares program, C.K. Johnson's ORTEP and locally written programs. All computational work was performed on the CDC-Cyber 170/760 at the State University Data Center and CSULA.
19 D.T. Cromer, and J.T. Waber, International Tables for X-Ray Crystallography; Kynoch Press, Birmingham, England, 1974, Vol. IV, Table 2.2A, D.T. Cromer, ibid., Table 2.3.1.